Demonstration of Tokamak Discharge Shutdown with Shell Pellet Payload Impurity Dispersal

E. M. Hollmann, P. B. Parks, D. Shiraki, N. Alexander, N. W. Eidietis, C. J. Lasnier, and R. A. Moyer

Phys. Rev. Lett. **122**, 065001 — Published 12 February 2019

DOI: 10.1103/PhysRevLett.122.065001

Demonstration of Tokamak Discharge Shutdown with Shell Pellet Payload Impurity Dispersal

E.M. Hollmann[1], P.B. Parks[2], D. Shiraki[3], N. Alexander[2], N.W. Eidietis[2], C.J. Lasnier[4], and R.A. Moyer[1]

[1] University of California – San Diego, La Jolla, California 92093, USA
[2] General Atomics, San Diego, California 92186, USA
[3] Oak Ridge National Laboratory, Oak Ridge, Tennessee 37831, USA
[4] Lawrence Livermore National Laboratory, Livermore, California 94550, USA

The first rapid tokamak discharge shutdown using dispersive core payload deposition with shell pellets has been achieved in the DIII-D tokamak. Shell pellets are being investigated as a possible new path toward achieving tokamak disruption mitigation with both low conducted wall heat loads and slow current quench. Conventional disruption mitigation injects radiating impurities into the outer edge of the tokamak plasma, which tends to result in poor impurity assimilation and creates a strong edge cooling and outward heat flow, thus requiring undesirable high-Z impurities to achieve low conducted heat loads. The shell pellet technique aims to produce a hollow temperature profile by using a thin, low-ablation shell surrounding a dispersive payload, giving greatly increased impurity ablation (and radiation) rate when the payload is released in the plasma core. This principle was demonstrated successfully using outer diameter = 3.6 mm, thickness = 40 μm diamond shells holding boron powder. The pellets caused rapid (< 10 ms) discharge shutdown with low conducted divertor heat fluence (~0.1 MJ/m^2). Confirmation of massive release of the boron powder payload into the plasma core was obtained spectroscopically. Some evidence for the formation of a hollow temperature profile during the shutdown was observed. These first results open a new avenue for disruption mitigation research, hopefully enabling development of highly effective methods of avoiding disruption wall damage in future reactor-scale tokamaks.

Introduction. – Material ablation plays a crucial role in many fields including ultraviolet light sources [1], planetary science [2], astrophysics [3], and medicine [4]. In the area of magnetic fusion energy research, detailed studies of material ablation in plasmas could help design methods to prevent costly wall damage from major disruptions in future tokamak-based power plants. Major disruptions are global tokamak plasma instabilities which can result from control system failure or from crossing stability boundaries. Although extensive research has been devoted to avoiding disruptions [5, 6], it is doubtful that they can be avoided with 100% certainty, motivating the study of rapid shutdown methods to safely dissipate plasma energy in the event of an unavoidable disruption [7, 8].

All rapid shutdown methods being studied involve the injection of impurities to radiate away the plasma energy. Several impurity delivery methods have been studied, including gas injection, cryogenic pellet injection (PI), and shattered cryogenic pellet injection (SPI) [9]. Good progress has been made in understanding tokamak rapid shutdowns, with shattered neon pellet injection presently considered the most promising method for rapid shutdown of ITER [10].

Despite the progress made on rapid shutdown research, shortcomings persist in present methods, partially due to poor impurity assimilation resulting from edge deposition. Simultaneous reduction of induced vessel forces, conducted heat loads, and runaway electrons is challenging: higher-Z impurity injection tends to improve radiation efficiency, thus reducing conducted heat loads; but also causes more rapid electron temperature collapse (TQ) and more rapid current decay (CQ), thus increasing runaway electron (RE) production and induced vessel forces [9].

The dispersive shell pellet (DSP) concept seeks to increase impurity assimilation via the rapid delivery of a dispersive payload to the core of the discharge. High pressure gas [11] and dust [12] have been considered as payloads. An outer shell is used to hold the payload together and protect it from ablation at the plasma edge. In the ideal DSP shutdown, the pellet reaches the plasma core with minimal perturbation to the plasma, then releasing its payload and causing an inside-out TQ with inward flow of thermal energy, giving the low conducted heat loads characteristic of high-Z shutdowns, but with the longer CQ and low induced vessel forces characteristic of lower-Z shutdowns, as predicted by magneto-hydrodynamic (MHD) simulations [13].

A central challenge of the DSP shutdown method is the shell design. Previous attempts to demonstrate the DSP technique used polystyrene shells, which were unsuccessful; either not burning through in the core (for thick-walled shells) or breaking during launch (for thin-walled shells) [14]. Here, first successful demonstration of DSP shutdown with core impurity dispersal is presented, achieved by use of diamond shells.

Experimental technique. – The experiments were performed on the DIII-D tokamak [15]. Medium-energy ($W_{th} \approx 0.8$ MJ) deuterium H-mode lower-single null plasmas were used. Figure 1(a) shows a schematic of the pellet launcher. The pellets are launched using helium propellant, which is then removed by two pumping ports. Initial pellet velocities of 80 – 250 m/s are measured with a light gate. Additional essential diagnostics, shown in Fig. 1(b), include spectrometers, a visible fast-framing camera, an infrared camera, a CO_2 interferometer, and photodiode arrays to measure total and soft x-ray (SXR) brightness. The shell pellets used here had 3.6 mm outer diameter and 40 μm wall thickness. The wall was made of chemical vapor deposited diamond. The payload was 21 mg of boron dust with 44 μm max outer diameter (OD).

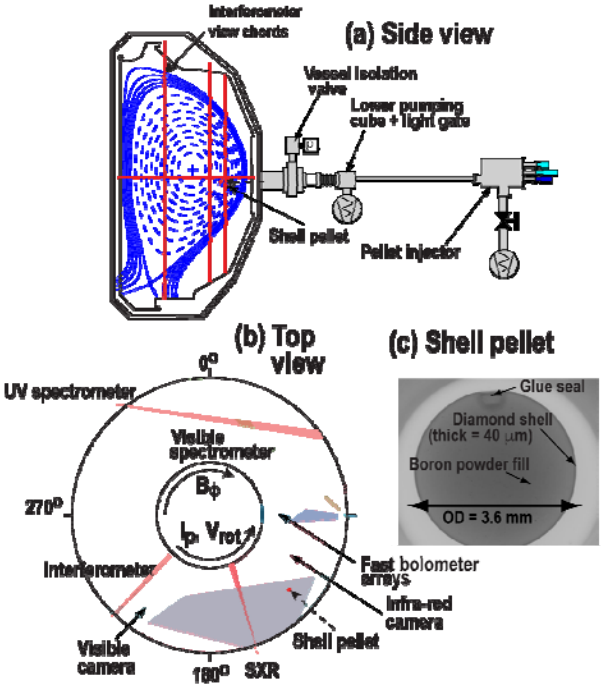

FIG. 1. (a) Schematic of pellet injector also showing equilibrium flux surfaces of target plasma; (b) tokamak top view showing key diagnostics; and (c) x-ray image of shell pellet.

Demonstration of shell pellet shutdown. – The main diagnostic used was the visible camera, which is operated with either B-II 412 nm (5 nm bandpass) or C-II 514 nm (4 nm bandpass) interference filters. Figure 2(a-h) shows visible images (with B-II filter) at different time steps, , were is the time at which first light from pellet-plasma interaction is observed. It can be seen that the pellet trajectory is fairly close (within ~ 1 cm) of the expected straight-line vacuum trajectory (dashed line), allowing an estimate to be made of the pellet minor radius, = r/a, Fig. 2(i). The pellet light emission can initially be seen to be fairly localized to the pellet and to be extended along *B*, the magnetic field. In Fig. 2(e), however, a cross-field dispersal of material can be seen, interpreted as shell burn-through and boron dust release. "Burn-through" is used here in the sense of ionization out of the neutral state.

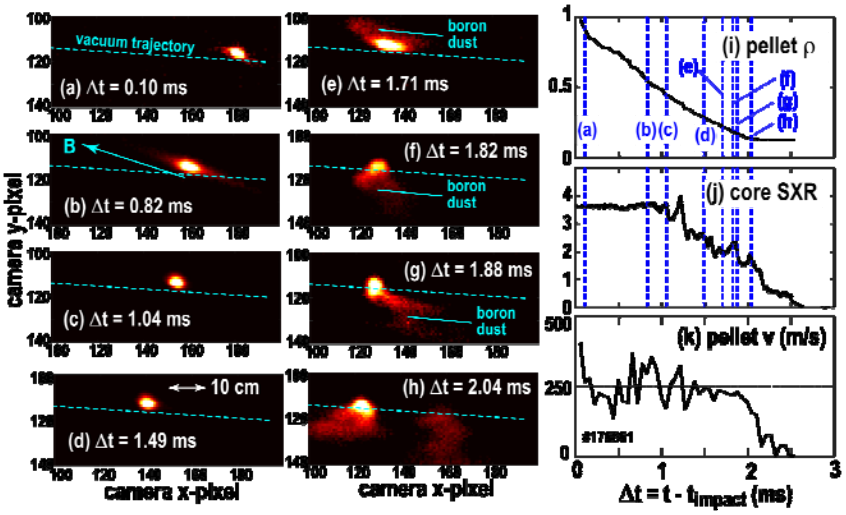

FIG. 2. (a-h). Visible images of shell pellet trajectory at different time steps, and (i) inferred pellet minor radius, (j) core SXR brightness vs time, and (k) inferred pellet velocity.

Figure 3 compares time traces of pellet burn-through with modeling for a pellet with initial velocity ~ 230 m/s. The pellet trajectory is shown in Fig. 3(a), showing that pellet shells appear to burn through at ~ 0.25, although pellet material goes farther, to ~ 0.15, before stopping. Pellet brightness (integrated spatially over the image) is shown in Fig. 3(b); B-II and C-II imaging (obtained from repeat shots) are similar, due to large levels of continuum emission. There are spikes in emission seen when the pellet crosses the $q = 2$ surface and again near the $q = 3/2$ surface. These spikes are not understood at present. Previous small (non-disrupting) pellets observed emission dips associated with thermal energy depletion on rational surfaces [16]. Strongly perturbing (disrupting) pellet experiments, however, exhibited emission spikes at rational surfaces, possibly from enhanced cross-field heat transport from instabilities [17]. The simulated pellet/payload trajectory is shown in Fig. 3(c), predicting shell burn-through around ~ 0.3. For this simulation, recent calculations for carbon and boron ablation rates are used [18]. Ablated material is assumed to be deposited on flux surfaces over the width of the pellet diameter, and resulting plasma cooling due to ionization, dilution, and radiation is calculated from CRETIN [19]. The effect of cross-field heat transport is checked using a new kinetic model [20] but is found to be small; for example, in the simulation of Fig. 3(c), including a radial thermal diffusivity of only increases shell penetration depth by = 0.015. After shell burn-through, the payload ablation is calculated in two limits: a solid boron limit, where the boron dust is treated as a single solid pellet of equivalent mass; and an isolated dust limit, where dust ablation is calculated as if every grain were exposed to the full plasma heat flux. As expected, B dust has a higher ablation rate, Fig. 3(d), but both B dust and solid B pass through the plasma without burning through. Within the scatter of the data, Fig. 2(k), shell pellet slowing is not observed and is therefore ignored. B dust slowing is observed, however; to match this, the ablation pressure gradient force on the dust needs to be increased by 3 , Fig. 3(c). This factor 3 is not understood at present, but could be due to interactions between dust grains, from ion

drag, or from electric field forces. The disappearance in dust signal at t ~ 2.5 ms is thought to occur because the TQ comes to an end, Fig. 3(g), reducing ablation. Experiments using solid plastic pellets of similar radius show that solid pellets of ~mm size can be observed even during the CQ, but it is likely that <40 m dust is not visible.

The plume radius is shown in Fig. 3(e). It can be seen that the plume is initially broader in C-II, consistent with line emission becoming dominant (relative to continuum) at the ablation plume edge. There is a rapid jump in plume radius which coincides with the observation of shell burn-through (dot-dashed vertical lines), suggesting that this jump is due to dust dispersal. Total radiated power measured at toroidal angles and are shown in Fig. 3(f). It can be seen that the radiated power is asymmetric toroidally. Figure 3(g) shows core SXR brightness and Fig. 3(h) shows plasma current. It can be seen that the TQ begins after the pellet crosses the q = 3/2 surface, and payload dispersal then occurs roughly in the middle of the TQ.

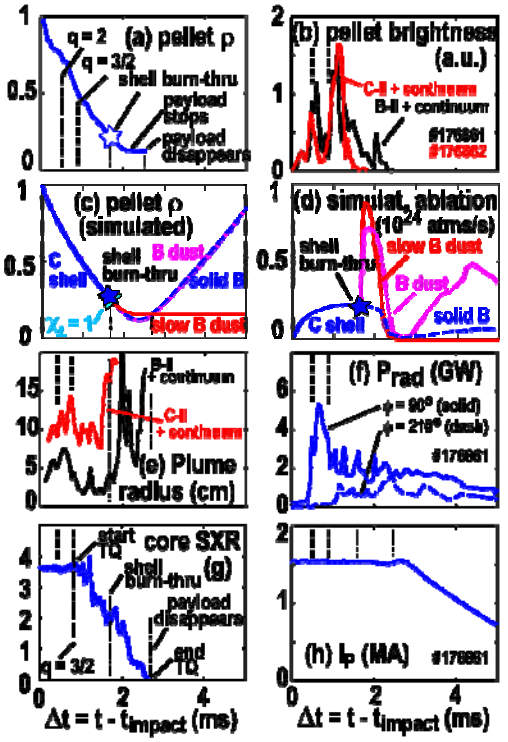

FIG. 3. Time traces of fast (v ~ 230 m/s) shell pellet shutdown showing (a) pellet minor radius, (b) ablation plume brightness, (c) simulated pellet minor radius, (d) simulated ablation rate, (e) ablation plume characteristic radius, (f) radiated power, (g) core SXR, and (h) plasma current.

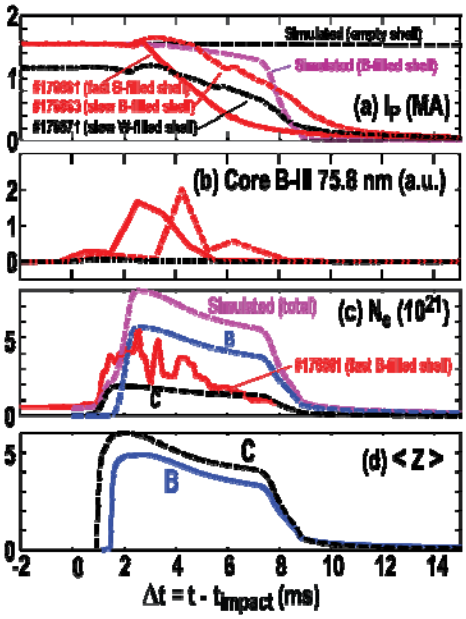

FIG. 4. Time traces of (a) plasma current, (b) core B-III line brightness, (c) total electron number for fast pellet with boron payload, and (d) mean charge state from 0D model.

Confirmation of boron dispersal in the plasma during the TQ is obtained spectroscopically. Figure 4(a) shows time traces of plasma current for three shots – red curves are boron-filled shell pellet shots with $v \sim 100$ m/s and $v \sim 230$ m/s, while the black curve is a $v \sim 100$ m/s tungsten powder-filled shell pellet. Core boron line emission rises before the CQ onset for the boron-filled pellets, Fig. 4(b), consistent with boron being released during the TQ. Figure 4(c) shows the total plasma electron number reconstructed from interferometers for the fast boron-filled pellet shot. The upper dashed curve shows the electron number simulated from 0D ionization/recombination modeling of the injected atoms (KPRAD) [21]. Individual contributions from C and B are shown by lower dashed curves. It can be seen that the predicted total electron number is about 2 higher than measured, possibly indicating that some of the boron persists in dust form during the CQ in the experiment, although toroidal asymmetries could also cause this. Figure 4(d) shows the mean charge states of B and C predicted by the 0D modeling. It can be seen that fully stripped ions are predicted during the TQ, with mean charge state dropping during the CQ. Figure 4(a) also shows simulated plasma current (from KPRAD) with and without the B payload included. Although these simulations are not expected to capture the precise details of the CQ (because current profile evolution is not included) the approximate CQ duration with B payload is much closer to the data than without B payload, supporting a strong effect on CQ dynamics by the payload.

Some preliminary evidence of an inside-out TQ forming during DSP shutdown was obtained from Thomson scattering data, shown in Fig. 5. In Fig. 5(a), it can be seen that the temperature profile is hollow at time = +1 ms. Due to significant jitter (of order 1 ms) in shell pellet arrival time, only this isolated example of a TQ profile was obtained. Additionally, the time = +1 ms is slightly prior to shell burn-through, so the hollowing does not appear to be due to the payload dispersal. However, this data does demonstrate that inside-out profiles are achievable, and can hopefully be made even more hollow (deeper) with less perturbing shells.

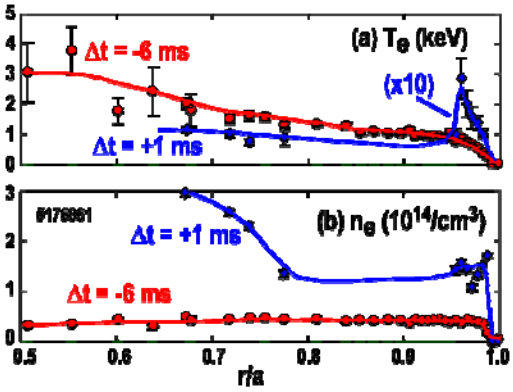

FIG. 5. Radial profiles of (a) electron temperature (with blue curve scaled 10) and (b) electron density measured before and after pellet impact.

Global characteristics.- An overview of typical disruption mitigation metrics are shown in Fig. 6 as a function of initial pellet velocity. Fig. 6(a) shows the height of the CQ spike, which is interpreted qualitatively as the degree of current flattening which occurs at CQ onset, and is therefore inversely linked to the level of TQ MHD. A low spike is desirable, as it indicates low MHD mixing of impurities and is associated with better impurity assimilation. CQ duration is shown in Fig. 6(b) - it can be seen that there is a clear decreasing trend in CQ duration with pellet velocity. This trend is undesirable, as it is desired to achieve long CQ duration with good heat load mitigation. Inner divertor leg heat fluence, from IR thermography, is shown in Fig. 6(c); this gives a qualitative picture of the degree of conducted heat load mitigation, showing excellent heat load mitigation (comparable to neon SPI). Integrated halo current amplitude is shown in Fig. 6(d); this gives a rough picture of the level of (undesirable) halo current vessel forces. Integrated CQ hard x-ray (HXR) signals are shown in Fig. 6(e); these reflect the level of (undesirable) runaway electron (RE) generation during the shutdown. Surprisingly, the DSP shutdowns can form REs, even with low Z injection, indicating very rapid cooling on good flux surfaces. The colored bands in Fig. 6(a-e) show approximate equivalent values for shutdowns with Ar PI, Ne SPI, and SPI. These are not for the same target plasma, being taken on different run days, so are intended for rough comparison only. Fig. 6(f) shows the estimated shell burn-through radius as a function of initial pellet velocity.

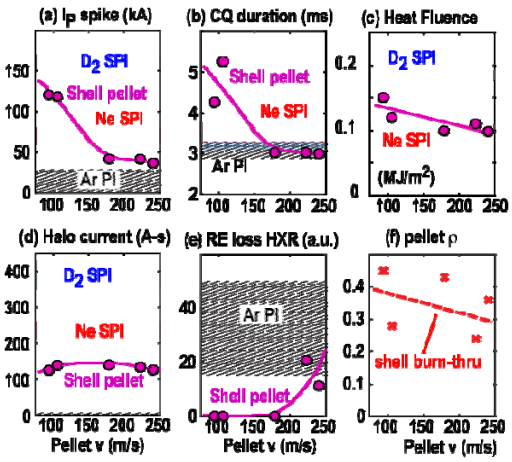

FIG. 6. Disruption mitigation metrics as a function of pellet initial velocity showing (a) spike height, (b) CQ duration, (c) inner strike point conducted heat fluence, (d) integrated halo current amplitude, (e) runaway electron prompt loss level, and (f) shell burn-through radius.

Summary and conclusion.- This work presents first demonstration of the shell pellet concept for tokamak disruption mitigation. This differs significantly from conventional disruption mitigation, where impurities are dominantly mixed into the plasma by MHD processes. Many encouraging features were observed, including core release of boron dust and evidence for rapid slowing of the dust payload after being released. Shell burn-through appears to occur close to the minor radius predicted by ablation modeling. Assimilation of injected material (shell + payload) appeared to be quite good (>50%). Low conducted heat loads, low spike, and low halo currents were observed at higher pellet velocities. Undesirable trends included strong plasma perturbation by the shell (indicating a need for even lower Z shells), toroidally localized TQ radiation, short CQ duration, and RE formation. Overall, the disruption mitigation characteristics of these prototype shell pellets are quite good, giving reason to believe that even better results can be obtained with future, more optimized, designs. Preliminary modeling work [18] indicates that the shell pellet concept is reactor relevant. Different shell pellets would need to be available depending on disrupting plasma conditions; but, as an example, penetration to the core ($r/a < 0.4$) of a full-power ITER plasma appears to be achievable with a OD = 1.5 cm Be pellet with an experimentally achievable velocity (v = 600 m/s). Future experiment/modeling comparisons will hopefully strengthen these preliminary findings.

The authors wish to thank L. Chousal, J. Kulchar, A. Horton, and D. Ayala for assistance with design, testing, and installation of the pellet injector and J. Herfindal, A. Lvovsky, I. Bykov, M. van Zeeland, F. Glass, Y. Zhu, and D. Thomas for diagnostic support and A. Hyatt, H. Torreblanca for operations support. This work was supported by the U.S. Department of Energy under Grants No. DE-FG02-07ER54917, DE-FC02-04ER54698, and DE-AC05-00OR22725. DIII-D data shown in this paper can be obtained in digital format by following the links at https://fusion.gat.com/global/D3D_DMP. **Disclaimer:** This report was prepared as an account of work sponsored by an agency of the United States Government. Neither the

References

[1] M.G. Su, Q. Min, S.Q. Cau, et al., Scient. Rep. **7**, 45212 (2017).
[2] M.D. Campbell-Brown and D. Koschny, Astron. Astrophys. **418**, 751 (2004).
[3] R.P. Drake, "High energy density physics," (Springer, New York, 2006).
[4] E. Schena, P. Saccomandi, and Y. Fong, J. Funct. Biomater. **8**, 19 (2017).
[5] J.A. Snipes, S. Bremond, D.J. Campbell, et al., Fus. Eng. Design **89**, 507 (2014).
[6] D. Humphreys, G. Ambrosio, P. de Vries, et al., Phys. Plasmas 22, 021806 (2015).
[7] E.M. Hollmann, G. Arnoux, N. Commaux, et al., J. Nucl. Mater. **415**, S27 (2011).
[8] M. Lehnen, K. Aleynikova, P.B. Aleynikov, et al., J. Nucl. Mater. **463**, 39 (2015).
[9] E.M. Hollmann, P.B. Aleynikov, T. Fulop, et al., Phys. Plasmas **22**, 021802 (2015).
[10] N. Commaux, D. Shiraki, L.R. Baylor, et al., Nucl. Fusion 56, 046007 (2016).
[11] E.M. Hollmann, A.N. James, P.B. Parks, et al., "Atomic Processes in Plasmas," AIP Conf. Proc. **1161**, 65 (2009).
[12] P.B. Parks, "Dust ball pellets for disruption mitigation," Invention Disclosure DOE Case no. S-113-472 (2007).
[13] V.A. Izzo and P.B. Parks, Phys. Plasmas **24**, 060705 (2017).
[14] E.M. Hollmann, N. Commaux, N.W. Eidietis, et al., Phys. Plasmas **17**, 056117 (2010).
[15] J.L. Luxon, Nucl. Fusion **42**, 614 (2002).
[16] W.A. Houlberg, S.L. Milora, and S.E. Attenberger, Nucl. Fusion **28**, 595 (1988).
[17] E.M. Hollmann, N. Commaux, R.A. Moyer, et al., Nucl. Fusion **57**, 015008 (2016).
[18] P.A. Parks, "The ablation rate of some low-Z pellets with a kinetic model for the degradation of the incident plasma electrons in the surrounding ablation cloud," to be submitted to Phys. Plasmas (2019).
[19] H.A. Scott, J. Quant. Spectrosc. Radiat. Transfer **71**, 689 (2001).
[20] P.A. Parks and E.M. Hollmann, "A kinetic model for plasma cooling induced by pellet injection," to be submitted to Phys. Plasmas (2019).
[21] E.M. Hollmann, P.B. Parks, and H.A. Scott, Contr. Plasma Phys. **48**, 260 (2008).